Technical Sciences
Academy of Romania
www.jesi.astr.ro

Journal of Engineering Sciences and Innovation
Volume 10, Issue 4 / 2025, pp. 407 - 430

C. Chemical Engineering, Materials Science and Engineering

Received ***17 August 2025*** *Accepted* ***10 December 2025***
Received in revised form ***14 October 2025***

Materials studies by Mössbauer spectroscopy

ION BIBICU*

Technical Sciences Academy of Romania, Bucharest, Romania

Abstract. Mössbauer spectroscopy is one of the different methods for the analysis of the phase composition and the microstructure of materials. The ^{57}Fe is the most studied isotope followed by ^{119}Sn and ^{151}Eu.The paper presents the studies on the different materials performed by Mössbauer spectroscopy. The studies were performed in the transmission and surface geometry and by Rayleigh scattering of Mössbauer radiation. Were studied the properties of the following materials: steels (Fe-Si electrotechnical steels: determination of internal magnetic field; Fe-C steels: study of surface, their corrosion in ammoniacal solutions and HCl solutions, the inhibition effect of some organic compounds, electrolytic galvanization; stainless steel 316L in biologic environment); ferities (Co ferrite preparation, Co ferrite in silica matrix, films from MnZn and NiZn ferrites); amorhous magnetic alloys ($Fe_{81}B_{13.5}Si_{3,5}C_2$, $Fe_{87}Zr_6B_6Cu_1$, $Fe_{62}Ni_{16}B_{14}Si_8$, $Fe_{80}B_{20}$); thin films from Cu and Ag doped with ^{57}Fe; Eu doped compounds (langasite crystals, yttrium aluminates garnets, YVO_4); chalcogenides ($SnSe_2$); semi-conducting oxides [$xSnO_2$-(1-x)αFe_2O_3]; etc.

Keywords: Mössbauer spectroscopy, Fe-Si steel, Fe-C steel, steel corrosion in ammoniacal media, corrosion in HCl solutions, corrosion inhibitors, Fe-C steel electrolytic galvanization, stainless steel 316L, ferities, amorphous magnetic alloys, thin films, Eu doped compound, chalcogenides, semi-conducting oxides.

1. Introduction

Mössbauer spectroscopy [1] (or nuclear γ resonance) is based on the incorporation of the emitting and absorbing nuclei within a solid matrix, which enables resonant recoil free absorption and emission of γ-rays. Its importance lies in the very narrow line width of the emitting photon resulting from the relatively long lifetime of the excited nuclear state - typically of 10^{-8} s, corresponding to a natural line width of the order of 10^{-8} eV - and the consequent ability to probe the variations in nuclear energy levels resulting from any discrete changes in the chemical state and/or environment of the Mössbauer nucleus. Such changes in nuclear energy levels are

*Correspondence address: ionbibicu10@gmail.com

measured by modifying the energy of the probing γ-rays by applying a Doppler shift; a Mössbauer spectrum therefore consists of a plot of counts against applied Doppler velocity (positive and negative), Significant recoil-free-fractions occur only for gamma energies less than 150 keV. For the collecting data it is necessary to do measurements at low temperatures as the energy of the gamma ray increases. Room or high temperature Mössbauer work is possible only for a limited number of elements: e.g. ^{57}Fe, ^{119}Sn, ^{151}Eu. Following resonant absorption of a gamma ray, the nucleus may de-excite by emission of a gamma ray or by the process of internal conversion where an inner (K or L) shell electron is emitted. Accompanying conversion electron emission is a characteristic X-ray emitted as a result of the repopulation of the inner energy levels. The detection of the three backscattered particles, permits surface studies to be performed. The electron signal is quite high for the ^{57}Fe, ^{119}Sn and ^{151}Eu isotopes. The normal transmission geometry investigates iron-containing samples of thickness typically < 30 microns. However, in scattering geometry surfaces coatings and thin films can be studied on substrates and to various depths through the detection of three backscattered radiations. From values of hyperfine interactions and recoil free fraction (f-factor) obtained it is possible to derive the phase analysis and the site population for the various sites in a specific phase. The ^{57}Fe is the most studied isotope followed by ^{119}Sn and ^{151}Eu. Mössbauer spectroscopy [2-4] has as one of its most important features the ability to simultaneously undertake bulk and surface analyses. It is a non-destructive technique that can be applied *in situ* to investigate surface of varying thickness from thin films to coatings without the need to remove them from their substrate. On the other, it suffers from a lack of sensitivity and for the very thin surfaces and interfaces take too long acquisition times. With the growing interest in nanomaterials, catalysis and corrosion the surface Mössbauer technique will be more widely used.

The paper presents the studies on: steels (Fe-Si electrotechnical steels; Fe-C steels: study of surface, their corrosion in ammoniacal solutions and HCl solutions, the inhibition effect of some organic compounds, electrolytic galvanization; stainless steel 316L in biologic environment); ferities (Co ferrite preparation, Co ferrite in silica matrix, films from MnZn and NiZn ferrites); amorhous magnetic alloys ($Fe_{81}B_{13.5}Si_{3,5}C_2$, $Fe_{87}Zr_6B_6Cu_1$, $Fe_{62}Ni_{16}B_{14}Si_8$, $Fe_{80}B_{20}$); thin films from Cu and Ag doped with ^{57}Fe; Sn compounds: Eu doped compounds (langasite crystals, yttrium aluminates garnets, YVO_4 crystals).

2. Studies of steels

Studies have been carried out on different types of steels: Fe-C, Fe-Si, stainless steel. These studies have followed different aspects: characterization of materials, study of corrosion processes in different environments, effect of corrosion inhibitors [5]. The measurements were carried out at room temperature in transmission and backscattering geometry

2.1. Material properties

In the studies of Fe-C steels the scope was to develop a study method for steel, method useful for a physical metallurgy laboratory and to determine hyperfine parameters for samples delivered by Hunedoara steel plant [6[. Were analyzed the following steel samples in the concentration range of 0,10-0,60 w%C: OLC-10 with 0.07 and 0.11 w%C, OLC-15 with 0.15 w%C, OLC-25 with 0.25 w%C, OLC-35 with 0.37 w%C, OLC-45 with 0.47 w%C, OLC-55 with 0.56 w%C OLC-60 with 0.59 w%C. The Mössbauer spectra were analysed with a computer fitting program for three magnetic sublattices. The following hyperfine parameters were determined: magnetic hyperfine splitting, electric quadrupole splitting and isomer shift. The values of the parameters are given in the Table 1 for all investigates samples. Mössbauer spectrum of the sample OLC-10 with 0.07 w%C is best fitted with a single magnetic lattice (single sextet) with parameters very closed to pure metallic Fe (≈ 331 KOe magnetic field). In the sample OLC-10 with 0.11 w%C we found a new sextet with lower magnetic field ≈ 317 KOe. The second sextet is present in all samples with higher C concentration. In the sample with 0.37 w%C concentration and higher is present a new sextet, the third, with magnetic field ≈ 160 KOe. The three observed sublattices can be attributed as follows: the sextet with the highest value of the magnetic hyperfine field, noted sublattice 1, can be attributed to Fe atoms with C atoms neighbouring of order 3 and 4 and Fe atoms no affected by the presence of C atoms; sublattice noted 2 corresponds to Fe atoms with C atoms neighbouring of order 1 and 2; sublattice noted 3, with the lowerest value of the magnetic hyperfine field represents a new compound: Fe_3C cementite.
Magnetic hyperfine field for the sublattice 2 does not depends of C concentration, showing that C atoms filled uniformly interstitial positions. The high value of the quadrupole spitting for cementite attested a significant distorsion of its network. After the cementite apparition, the C atoms do not enter in sublattice 2; C atoms enter preferably in cementite.
The use of Fe-Si alloys in electrotechnical industry as magnetic material has encouraged the investigations of this alloy for getting a better understanding of their physical properties. In our study [7] we proposed to use Mössbauer spectroscopy as a standard method of investigation in order to determine the magnetic fields for Fe-Si electrotechnical steels with low Si concentration (< 7.92 % Si). At the same time were discussed the results by means of the model of the variation of the spin polarization of the 4*s* –like electrons with distance from the iron atom. Fe-Si samples with Si concentration in the range 5.77 – 7.92% Si were prepared, measured and interpreted as Fe-C steel samples. From obtained data one can conclude the existence of three magnetic sublattices with values of the hyperfine magnetic fields of $H_1 \approx 334$ kOe, $H_2 \approx 310$ kOe and $H_3 \approx 279$ kOe.
These values do not depend on the Si cntent. The three observed sublattices can be attributed as follows: the sextet with the highest value of the magnetic hyperfine field, noted sublattice 1, can be attributed to Fe atoms with Si atoms neighbouring of order 4 and 5; sublattice noted 2 corresponds to Fe atoms which in 1 shell have

an iron atom replaced by a Si atom; sublattice noted 3 corresponds to Fe atoms which in 2 shell have two iron atoms replaced Si atoms.

Table 1. The values of determined hyperfine parameters

Steel	Isomer shifts [mm/s]			Quadrupole Splitting [mm/s]			Hyperfine Fields [KOe]		
Sublattice at % C	1	2	3	1	2	3	1	2	3
Pure metallic Fe	0.226 ±0.01			0			331.1 ±0.03		
OLC-10 0.07	-0.22 ±0.03	-	-	0.00 ±0.03	-	-	326.4 ±0.9	-	-
0.11	-0.23 ±0.03	0.03 ±0.03	-	0.04 ±0.03	0.01 ±0.03	-	327.8 ±0.9	315.9 ±1.1	-
OLC-15 0.15	-0.23 ±0.03	-0.21 ±0.03	-	0.00 ±0.03	0.03 ±0.03	-	328.8 ±0.9	316.7 ±2.5	-
OLC-25 0.25	-0.25 ±0.03	-0.21 ±0.03	-	0.02 ±0.03	0.00 ±0.03	-	331.4 ±0.9	320.0 ±0.9	-
OLC-35 0.37	-0.25 ±0.03	-0.23 ±0.03	0.23 ±0.03	0.00 ±0.03	0.02 ±0.03	0.58 ±0.06	333.0 ±0.3	321.0 ±1.1	179.5 ±2.7
OLC-45 0.47	-0.24 ±0.03	-0.22 ±0.03	0.43 ±0.05	0.00 ±0.03	0.03 ±0.03	0.62 ±0.04	331.0 ±0.4	320.4 ±0.9	155.7 ±4.1
OLC-55 0.56	-0.24 ±0.03	-0.22 ±0.03	0.41 ±0.05	0.02 ±0.03	0.00 ±0.04	0.62 ±0.09	329.3 ±0.9	314.6 ±5.8	156.9 ±4.0
OLC-60 0.59	-0.23 ±0.03	-0.20 ±0.03	0.45 ±0.03	0.00 ±0.03	0.00 ±0.03	0.60 ±0.03	331.5 ±0.9	319.0 ±1.4	156.5 ±2.2

Our results confirmed the hypothesis of the polarization of conduction electrons caused by the spin and charge perturbation of the 4*s* band of iron due to the interaction with the excess charge of the Si impurity atoms. The independence of the isomer shifts on silicon content may be explained by the screening of the excess charge of Si atoms by 4*s*-like electrons.

2.2. Corrosion of steels

Under ambient conditions a metallic material forms compounds by reactions with the medium contacted. While “corrosion” describes the degradation of a material by chemical reactions with the surrounding medium, in particular “rusting” describes the corrosion process of iron-based materials by reactions with water or humid air including the presence of solved and polluted solvents [8]. Natural corrosion is, most commonly, an undesirable process by which many metals with positive or slightly negative oxidation potentials are transformed into their chemical compounds. Well-known and particularly damaging to the economy is the rusting of iron. To understand and to reduce the corrosive attack on metallic materials is an important task from economical point of view.
Corrosion studies were performed on low-alloyed carbon steel samples or stainless steel samples used in biological media. The media used in the studies were:

ambient atmosphere, diluted ammonia/ammonium solutions, dilute HCl solutions, physiological environments. [9]

I performed the first study on corrosion by Mössbauer effect at the suggestion of professor of physics from my faculty, Prof. Dr. G. Moisil [10]. This first study, carried out in the transmission geometry, showed that in order to obtain relevant and precise data it is necessary to carry out surface studies. Thus, over time, detectors were made for surface studies through the Mössbauer effect and then I made various collaborations for Mössbauer surface measurements.

2.2.1. Corrosion products formed on a sample after storage in the ambient atmosphere

The surface of low-alloyed carbon steel sample was studied after storage in the ambient atmosphere [11]. Mössbauer effect measurements were performed in two geometries: transmission (TMS) and backscattering. An absorber from surface of the sample was obtained by scrapping. Information about samples surfaces was found by detecting the conversion electrons (CEMS) and the conversion X-rays (CXMS). The electrons penetration depth is of the order of 250 nanometers and the X-rays penetration depth is of the order of 11 microns [μm]. The backscattering measurements were conducted at a high degree of accuracy with a new detector, gas-flow proportional [12].

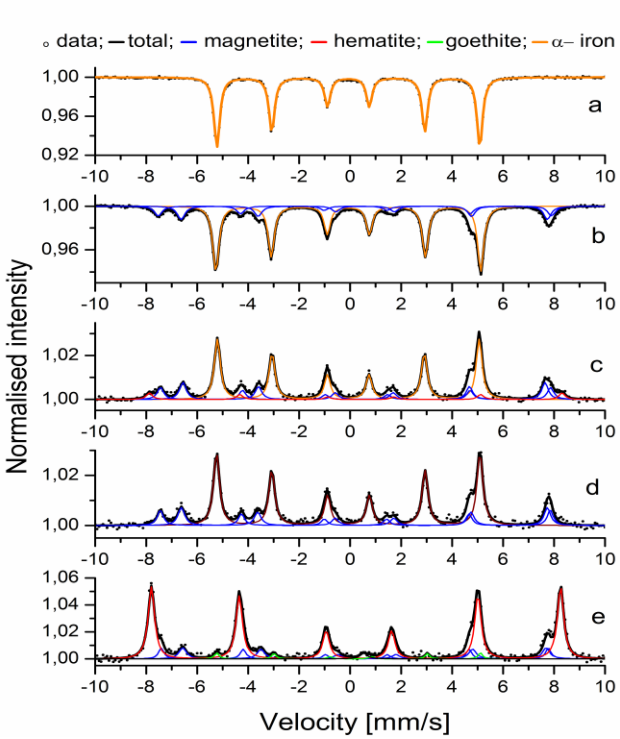

Fig. 1. Mössbauer spectra of the stocked sample (a) from bulk; (b) of surface scrapped layer; (c) by CXMS without filter; (d) by CXMS with filter; (e) by CEMS.

Figures 1 show the Mössbauer spectra of the sample togheter with the computer fit (continuous lines). The bulk transmission (Fig. 1a) spectrum was fitted with a single sextet due low carbon content. The surface measurements prove a marked corrosion: a coating with a considerable thickness and a complex composition. Hematite is the main compound of the outermost layer (Fig. 1e). Its Mössbauer parameters are practically the same with those given in literature. The second compound in the outermost layer is magnetite with a normal stoichiometry as in different references. The reduced hyperfine magnetic field of goethite compared with well-crystallized goethite (around 380 kOe), can be generally assigned to varying crystallinity of goethite and/or small particles. Also a corrosion product can exist in the outermost layer at sensibility limit of the method. Its presence is suggested by smoothing the spectrum. CEMS spectra indicate a corrosion layer thickness greater than 250 nm. The spectrum of steel substrate was not evidenced. The surface spectra obtained by CXMS without electron filter (Fig. 1c) give the integral information about superficial corrosion layer. The magnetite and hematite are the compounds of the layer. Magnetite is now the main compound of the corrosion layer. The using of the electron filter hides the hematite presence (Fig. 1d). Also the hematite is not present in the surface sample collected by scape method (Fig. 1b). The data obtained for sample collected by scape method are very closely to those obtained by CXMS with electron filter. All CXMS spectra evidenced the steel substrate. The compounds of the corrosion layer are: magnetite, hematite, and goethite. The relative concentration in increasing order is: goethite, hematite, and magnetite. The goethite and hematite are located at the surface of corrosion layer. We estimated the corrosion layer thickness around 5 microns.
The X-ray diffractograms of the sample confirm the Mössbauer data.

2.2.2. Corrosion of steels in ammoniacal media, inhibition effects

Researchers have commonly ignored the industrial and residual waters containing ammonia/ammonium regarding them as non-dangerous in terms of corrosion. Relatively recent researches, however, have showed such waters have a negative impact on the environment leading to pipe corrosion in the cooling waters systems, especially in the ammonium fertilizer industry.
The samples were corroded in a standard electrolytic cell with the followings diluted ammonia/ammonium solutions: diluted ammoniac solutions with NH_3 concentration of 10^{-1} M, 10^{-2} M, 10^{-3} M and 10^{-4} M [13], ammonium salts solutions: 0.1M NH_4Cl, 0.1M NH_4Cl with 0.05M NH_4NO_3,[14], solution 10^{-3}M NH_3 with 510^{-3}M NH_4Cl [14]. The CEMS spectrum of the sample corroded in solution with 10^{-3} NH_3 concentration [13] is shown in figure 2. The best fit of the CEMS spectrum for the corroded sample uses an addition Fe^{3+} paramagnetic doublet to the sextet. The parameters of the sextet are almost identical to those of the non-corroded sample. The slight changes of the hyperfine magnetic values and isomer shifts suggest that in the process of corrosion there may be a certain preference for the positions of iron, which are no close to the atoms of the alloying elements. The preferential orientation of the magnetic moments in the sample plane continues to

exist even after the corrosion of the samples. The main difference between the corroded sample sextets and the non-corroded sextets consists in the decrease of the intensity lines corresponding to α-Fe. This demonstrates, once again, the presence of a superficial layer on the corroded samples surface.

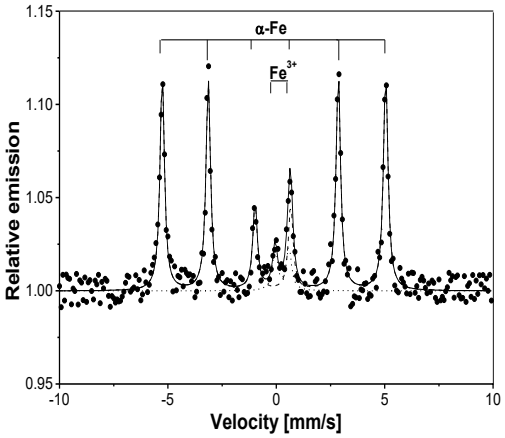

Fig. 2. CEMS spectrum of a Fe-C steel sample corroded in a solution with 10^{-3} NH_3 concentration (• data; — fit; ⋯ Fe^{3+}; --- α-Fe).

There is a process of inhibition of carbon-steel corrosion in the ammoniac solutions, which is evidenced by the increase of the superficial layer when NH_3 concentration decreases. The parameters of the doublets show the presence of Fe^{3+} and are similar to those shown by amorphous Fe^{3+} oxyhydroxides, superparamagnetic α-FeOOH and/or γ-FeOOH and $Fe(OH)_3$. Small relative area of the doublet, as well as its parameters shows the initial stage of the corrosion. At this stage we believe that the main product of the corrosion in NH_3 solution is an amorphous Fe^{3+} oxyhydroxide with a non-stoichiometric composition. Mössbauer data showed that for the samples corroded in ammonium salts solutions the main corrosion product is a mixture of Fe(III) ferrihydrate and FeOOH (alpha and/or gamma). The introduction of NO_3^- anion in a solution of 0.1M NH_4Cl in NO_3^-/Cl^- = 1/2 ratio has an inhibiting effect by decreasing the expansion rate of generalized corrosion of carbon steel. This effect is demonstrates by the increase of the sextet lines intensity and the dramatic decrease of the Fe^{3+} paramagnetic doublet.

Numerous advanced treatments using organic compounds have been proposed in order to improve the corrosion protection. The inhibition effect of three organic compounds: 2-mercapto-benzothiazol (MBT) [16], N-ciclohexil-benzothiazole-sulphenamida (NCBSA) [17] and etilentiouree (ETU) [18] on the corrosion of carbon-steel in diluted ammonia /ammonium solutions at room temperature were studied. The CEMS spectrum of a corroded sample in a solution with 10^{-3} HN_3 concentration with 250 pap NCBSA inhibitor is presented in figure 3.

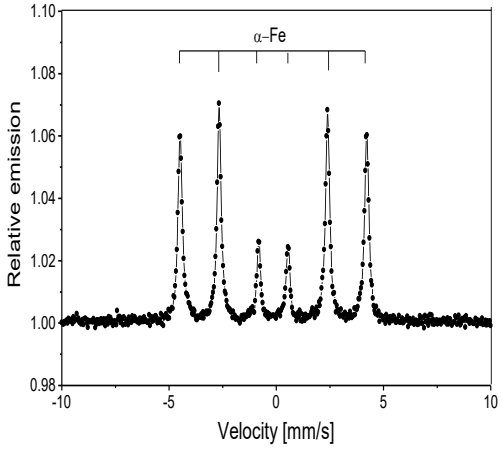

Fig. 3 CEMS spectrum of a corroded sample in a solution with 10^{-3} HN_3 concentration with NCBSA inhibitor (● data; — fit; --- α-Fe).

The similar spectra are obtained for MBT and ETU inhibitors. In these spectra there is no evidence for any iron corrosion product at the surface. A relative decrease of the α-Fe line intensities as compared with the sextet obtained in the corrosion process without inhibitor indicated formation of a superficial layer. Also the increased magnetic anisotropy of the CEMS spectra in the presence of the inhibitors confirms the action of the inhibitor. The inhibition action was presented by a formation of a superficial film without iron compounds on the surface of the corroded samples. This layer is interpreted in terms of the formation of complexes between inhibitors and the metal cations present in the carbon-steel structure. The data indicate a good absorbability of inhibitor on the metal surface.

2.2.3. Corrosion in dilute HCl solutions, inhibition effects

HCl acid solutions are widely used in industry, the most important fields of application being acid pickling, industrial cleaning, acid decaling, oil-well acid in oil recovery and the petrochemical processes. One of the most aggressive media for the ferric materials is the aqueous solution of hydrochloric acid. To understand and to reduce the corrosive attack on metallic materials is an important task from economical point of view.

The samples were immersed in a closed system for 3h in solutions of 1 M HCl [19] or 2 M HCl [20], [21]. The spectrum of the sample corroded in 1 M HCL is presented in figure 4. The best fit of the CEMS spectrum uses addition of two Fe^{3+} paramagnetic doublets to the sextet. The parameters of the doublets show the presence of Fe^{3+} and are similar to those shown by nonstoichiometric Fe^{3+} oxyhydroxides. The superficial layer consists of a mixture of α, β and γ-FeOOH. The superficial layer is thicker for sample corroded in HCl solutions then those corroded in ammonia media. In the 2 M HCl solution the corrosion layer is thicker than the layer formed in the corrosion in 1 M HCl solution and with the same

superficial compounds.

The importance of inhibition is much greater in solutions of hydrochloric acid since iron and its alloys are the most exposed materials both in industrial and other media. The inhibition effect of five organic compounds for samples corroded in solutions of HCl solutions were investigated: ammonium polymolybdate (APM) [19], n-acetyl p-aminobenzene sulfonamide (APAS) [20] N-(2hydroxybenzilidene) thiosemicarbazide (HBTC) [21], Bis (benzothiazolyl) disulphide (BTD) [22] and 2-(cyclohexylaminomercapto) benzothiazole (CMB) [23]. All tested inhibitors operate in the same manner. The process of corrosion is considerable slowed in the inhibitor presence and a superficial compound of Fe^{3+} without a magnetic arrangement is formed. The diminution of the corrosion process is indicates by the increased magnetic anisotropy of the CEMS spectra in the presence of the inhibitors. This means that the depth of the corroded surface layer is lower in the inhibitor presence or corrosion velocity diminished.

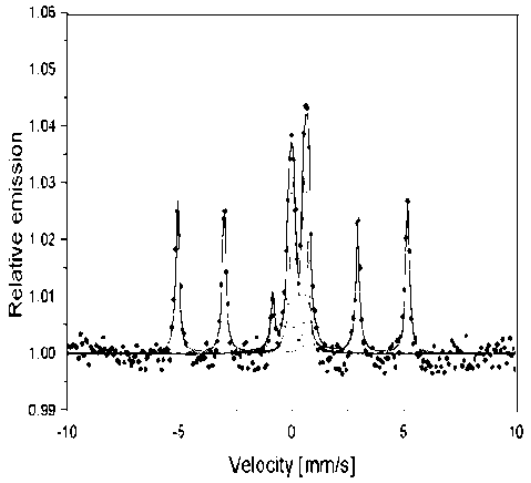

Fig. 4 CEMS spectrum of a corroded sample in a 1 HCl solution
(● data; — fit; -o- α-Fe; -Δ- doublet 1;-∇- doublet 2)

By estimating the relative area of the superficial compound and the increased magnetic anisotropy of the CEMS spectra in the presence of the inhibitors, results that the compound has a smaller thickness or, in extreme case is similar with the layer formed in the corrosion process without inhibitor. The Mössbauer parameters of the compound in this case do not differ too large from the ones found for the corroded sample in the solution without inhibitor. The new parameters can be ascribed to nonstoichiometric compounds as well as to low crystallinity, *e.g.* ferrihydrates. We consider that the organic inhibitors used in HCl solutions act as an incipient "rust transformer" and favours the formation of a "superficial closed layer". These inhibitors transform some constituents of rust into corrosion inhibiting oxide phases. For the corroded samples in a solution of 2M HCl, the inhibition process is the same as in 1M HCl solutions.

2.2.4 Corrosion of stainless steels in biological media

The studies have been made in order to determine the corrosion reactions, which are necessary for foreseeing the behavior of the materials used in implantology in different conditions, in our case 316L stainless steel, a large used material. The passivation behavior of orthopedic implant was studied as a function of type of physiological media: glucydic, proteic and lipidic. Thus the electrochemical behavior of steel was studied in three artificial media: aminosteryl, intralipid and kabiven [24]. A standard electrochemical cell has been used to study the effect of artificial media. The best fitting of the spectra show the presence of a single line, typically for stainless steel, which is paramagnetic at room temperature. Mössbauer spectrometry confirms and endures the uniformity, compactness and stability of superficial passive film with the possible exception of some iron vicinities where the superficial layer was affected thus showing the presence of pits. The parameters of the lines are the same, within experimental errors, as for a reference sample. This proves the corrosion resistance of used stainless steel in the tested conditions.

In other study the behavior of 316L stainless steel in physiological serum was discussed [25]. A standard electrochemical cell has been used to study the effect of the serum. Transmission [TMS] and electron conversion spectroscopy [CEMS] spectra were performed on uncorroded test sample and on sample corroded in a serum solution. All spectra (TMS and CMS) show a central broad line, typical for austenitic stainless steels. The best fitting of the spectra was obtained for single line. The parameters of this line of the CMS spectra are the same within experimental errors excepting the effect. This means that the surface was, practically, insignificantly changed during the corrosion process. Mössbauer measurements do not point out micro-structural changes in the investigated samples. The effect decreased slowly for sample corroded in serum proving the presence of the thin superficial layer on corroded sample. The Mössbauer spectroscopy proved, thus, the uniformity, compactness and stability of the surface passive films.

We studied the surface situation of 316L stainless steel sample implanted in a femur for 1 year [26]. The TMS and CEMS spectra were obtained for uncorroded sample and implanted sample. All spectra (TMS and CMS) show a central broad line, typical for austenitic stainless steels. The best fitting of reference sample spectrum was obtained for a single line. For the sample implanted spectrum the goodness of the fit impose two line variant. The relative areas of the two lines were: 27% and 73%. It was clear that during implantation a change in the superficial microstructure took place and a corrosion process was presently. Another difference between the reference sample and implanted sample consisted in a decrease of the intensity line for implanted sample. This proved the presence of thin superficial layer on implanted sample. We believed, inspired by references, that surface layer consisted mainly of oxide species. A slight improvement of goodness of the fit, within experimental errors, was obtained for implanted sample by using a sextet line near two lines. This fact suggests a possible apparition, in a small proportion of a martensitic phase on surface.

3. Ferrites

Ferrites are part of the large class of ferrimagnetic substances. Ferrites are the most widely used and known as materials with high magnetic permeability, obtained at affordable costs. In addition, some ferrites show sensitive dimensional changes, due to the phenomenon of magnetostriction, when an external magnetic field is applied to them; a typical case is cobalt ferrite. Depending on the shape of the magnetization hysteresis curve and the values of the main magnetic characteristics, the following ferrites are distinguished: soft magnetic ferrites (with a typical spinel or perovskite crystal structure) and hard magnetic ferrites (with a hexagonal crystal structure). Ferrites used industrially are synthetic, polycrystalline ceramic materials, obtained by sintering. Among the soft magnetic oxide systems, the most widely used are: $CoFe_2O_4$, $MnFe_2O_4$, $NiFe_2O_4$, $ZnFe_2O_4$, $MgFe_2O_4$, Cu Fe_2O_4, $NiFe_2O_4$, $Mn_{1-X}Zn_XFe_2O_4$, $Ni_{1-X}Zn_XFe_2O_4$.

First were studied the magnetic properties of NiZn and MnZn ferrite films deposited by laser ablation [27] Manganese-zinc ferrites are used in power electronics applications, (e.g. cores for chopper transformers in power supplies) and nickel-zinc ferrites used in high-frequency electronic applications, up to 800 MHz (e.g. cores for coils in radio communications and telecommunications). Magnetic behaviour of the films was studied comparatively to that of the bulk material. Mössbauer hyperfine field for films are close to those found for the bulk. Laser ablated films exhibit a higher coercive films field, which is explained in terms of the crystallite size distribution, with average values of 300-600 nm, as estimated from Mössbauer line broadening. A satisfactorily qualitative explanation of the magnetic properties is obtained on taking of the both the intrinsic properties and the extrinsic properties.

The following efforts were concentrated on preparation of Ni-Zn ferrite [28] Co ferrite [29-31] and Co ferrite nanocomposite [6]. The sintering properties of Ni-Zn ferrite with Cu substitution are significantly influenced by the copper content and sintering temperature [28]. This research indicates that the addition of copper can lower the sintering temperature required for achieving desirable properties. However, copper substitution can also negatively impact electrical resistivity, making optimization of the copper content crucial for high-frequency applications. In essence, the research highlights the interplay between sintering temperature, copper substitution, and the resulting properties of Ni-Zn ferrite. Careful control over these parameters is essential to achieve the desired characteristics for specific applications.

In the last decades cobalt ferrite was intensely studied thanks to magnetostriction properties useful for applications. The influence of two synthesis method (the conventional ceramic procedure and a wet method) on microstructural characteristics and magnetic properties of stoichiometric and manganese substitution cobalt ferrites was investigated [29]. The chemical route and/or sintering process influence microstructure characterized by lattice parameter, phase content, average grain size and the porosity. The best candidate for

magnetoresistive sensors are the manganese substituted Co ferrite samples characterized by lower values of the Curie temperature despite lower values of magnetorestrictive coefficients.
A study showing the correlation between chemical compositions, microstructural and magnetic properties of Co ferrite at different temperature were effected [30]. Four categories of samples were considered: stoichiometric cobalt ferrite, cobalt ferrite with excess of iron, cobalt ferrite with manganese, cobalt ferrite with silicon substitutions. The cobalt ferrite samples were synthesized using high temperature ceramic method. Cobalt ferrite studied in the paper demonstrates the sensitivity of magnetic and magnetostriction properties on the chemical composition and the parameters of sintering process. Samples with composition $CoFe_2O_4$ and $CoFe_{1.8}Mn_{0.2}O_4$ have the best ensemble of magnetic and magnetostrictive properties useful for sensor applications.

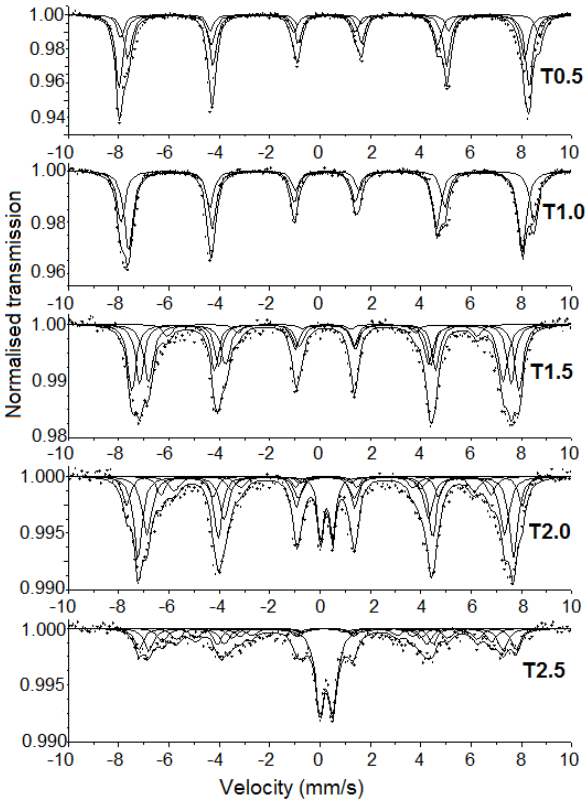

Fig. 5. Mössbauer spectra of x=0.5, x=1.0, x=1.5, x=2.0 and x=2.5.

Nanoscale ferrites represent a class of inorganic materials that has been intensively studied due to their diversity, the large number of synthesis methods and specific applications. The remarkable properties of these nanocrystalline magnetic materials arise from magnetic phenomena that occur at the nanoscale and that are different from those of bulk materials. For example, nanomaterials of the $Co_xFe_{3-x}O_4$ type

with controlled size exhibit electromagnetic absorption/shielding properties. The number of specialized publications describing the production and exploitation of nanoferrites is remarkable. Magnetic nanoparticles of $Co_xFe_{3-x}O_4$ (x = 0,5 – 2.5) were synthesized by redox reaction calcinations at 1000 ^{0}C using variable Co/Fe ratio [31]. The Mössbauer spectra, given in figure 5 are very similar to the spectra of cobalt ferrite described in literature. The Mössbauer spectrum of x=0.5 indicates the presence of hematite (α-Fe_2O_3) in addition to the spinellic phase. The two subspecta corresponding to Fe^{3+} in tetrahedral (A) and octahedral coordination (B) in spectrum of x=1.0 confirm the formation of cobalt ferrite, and the Mössbauer fit parameters are close to the bulk values. At higher x values, Mössbauer spectra show an increase in the line width and some "kinks" because-each subspectrum of the spinel phase is a combination of two or three sextets. The hyperfine fields at Mössbauer nucleus in both A and B sites gradually decrease with the increase of cobalt concentration as a result of cobalt substituting iron process in the spinel structure. An additional doublet with increasing intensity is present in case of x=2.0 and x=2.5 samples. The quadrupole doublet indicates the presence of paramagnetic ferrite. It is known that Curie temperature (Tc) of the $Co_xFe_{3-x}O_4$ decreases with the increase of the cobalt content. Also CoO appears at x=2 and x=2.5.

Recently, much attention has been focused on ferrite nanocomposites due to their improved optical, electronic and magnetic properties compared to those of single component nanomaterials. Therefore, silica coating of magnetic nanoparticles is becoming a promising approach in the development of nanocomposites for both fundamental and technological research. The SiO_2 matrix acts as a buffer and controls the particle size and prevents or decreases the agglomeration of magnetic particles. The key to obtain nanoscale single-phase spinel structure with enhanced magnetic properties of nanocomposites depend on SiO_2 content and annealing temperature. We studied the magnetic properties of $xCoFe_2O_4/(100\text{-}x)SiO_2$ nanocomposites by transmission Mössbauer spectroscopy at room temperature [32]. Magnetic spinel phase $CoFe_2O_4$ embedded in silica matrix indifferent molar ratios was obtained by sol-gel method, followed by annealing at 1100^{o}C. The variation of nanocomposite properties was studied for different molar ratios $CoFe_2O_4$:SiO_2 (10:90; 30:70; 50:50, 70:30 and 90:10, respectively). Mössbauer parameters obtained by fitting the spectra with Lorentzian line shape are given in Table 2. The spectra of the samples G30-G90 are similar to the spectra of cobalt ferrites from other composites obtained by other methods and described in literature and can be deconvoluted in two sextets. The two sextets show the presence of the cobalt ferrite. The two sextets corresponding to Fe^{3+} in tetrahedral (A) and octahedral coordination (B) in the spectrum of G90 confirms the formation of cobalt ferrite and the Mössbauer fit parameters are close to the bulk values. In cobalt ferrite structure Fe^{3+} ions and Co^{2+} ions can occupy both tetrahedral A and octahedral B site. The observed isomer shift (IS) supports the presence of iron in a 3+ valence state only. In spinel ferrites a larger isomer shift is expected at octahedral (B) sites as compared with tetrahedral (A) sites. The spectra of the

samples G30-G70 consist mainly in a superposition of two sextets. The large line in the central part of the spectra could be associated with paramagnetic contributions. At G10, Mössbauer spectrum exhibits large line widths and the subspectrum corresponding to tetra coordination is a combination of two sextets. The proportion of paramagnetic component increased and the huge quadrupole doublet can be associated with the formation of some silicate phase. The hyperfine fields at Mössbauer nucleus (H) in both A and B sites gradually decrease with the increase of SiO_2 concentration. Mossbauer studies indicate that Fe^{3+} and Co^{2+} occupy tetrahedral and octahedral sites. The degree of crystallinity increase with increasing $CoFe_2O_4$ content in silica matrix. Due to their magnetic properties, the nanocrystallites of $CoFe_2O_4$ embedded in the silica matrix, could be a promising solution for medical applications such as magnetic thermo-drug delivery.

Table 2. Mössbauer parameters of $xCoFe_2O_4/(100-x)SiO_2$ nanocomposites

Sample	X	H (kOe)	Δ (mm/s)	IS (mm/s)	A (%)	Site
G90	90	494,4	0,00	0,26	77,6	A-Tetra
		504,7	0,10	0,55	22,4	B-Octa
G70	70	486,5	0,02	0,30	86,5	A-Tetra
		509,0	0,11	0,47	11,7	B-Octa
		-	-	0,22	01,8	-
G50	50	483,5	0,00	0,30	89.7	A-Tetra
		505,5	0,12	0,46	08,3	B-Octa
		-	-	0,18	02,0	-
G30	30	477,5	0,02	0,30	90,3	A-Tetra
		503,0	0,13	0,49	05,6	B-Octa
		-	-	0, 16	04,0	-
G10	10	467,8	0,05	0,27	53,9	A-Tetra
		395,4	0,04	0,27	22,6	A-Tetra
		487,8	0,16	0,40	05,9	B-Octa
		-	2,84	1,28	10,1	
		-	-	0,26	07,5	
Errors		*± 2.5*	*± 0.04*	*± 0.02*	*± 2.5*	

4. Fe based amorphous magnetic alloys

Fe based amorphous magnetic alloys are of continuing interest as precursors of soft magnetic materials. These alloys can be produced by different methods. The alloys are of interest for in relation to their structural properties and many technical applications after suitable treatments and exposure to nuclear radiations. Were studied by Mösbauer spectroscopy and other methods structural and magnetic properties of the following amorphous magnetic alloys: $Fe_{81}B_{13.5}Si_{3,5}C_2$, (Metglass 2605 SC) [33-37], $Fe_{87}Zr_6B_6Cu_1$ [38], $Fe_{80}B_{20}$ [39], $Fe_{62}Ni_{16}B_{14}Si_8$ [40]. Metglass 2605 SC was the most researched substance.

It has been pointed out in literature that in the temperature range before any crystallinity could be detected in any amorphous ribbon, a chemical short-range

order is growing during annealing. We evidenced these changes in structure which influence the magnetic properties before material becomes crystalline for amorphous substance $Fe_{81}B_{13.5}Si_{3,5}C_2$, (Metglass 2605 SC) [33], [34], [35], [36]. The annealing process has been performed using 54,8 MHz rf exposure of amorphous $Fe_{81}B_{13.5}Si_{3,\ 5C2}$ ribbon sample. The ribbon samples of 30 μm thickness have annealed for equal time intervals to magnetic field directed within the ribbon plane. The pulse train frequency was 2.5 Hz and the puls3e width 10^{-1} s. and rf power values from 1 to 25 W were applied to different sample of the set. Room temperature TMS and CEMS [33], [34], [35] spectra or room temperature TMS, CEMS and CXMS spectra [36] of the annealed samples, showing no trace of a crystalline X ray diffraction pattern and surface oxides on have been recorded. The surface effects have been referred to the bulk behavior. From spectra were obtained quadrupole pattern and distribution of hyperfine fields. In figure 6 are presented CEMS, CXMS and TMS spectra and their hyperfine distribution after rf exposure to radiofrequency power (P_{rf}) of 25 W. These dates were analyzed in terms of of the atomic short-range ordering of the amorphous state.

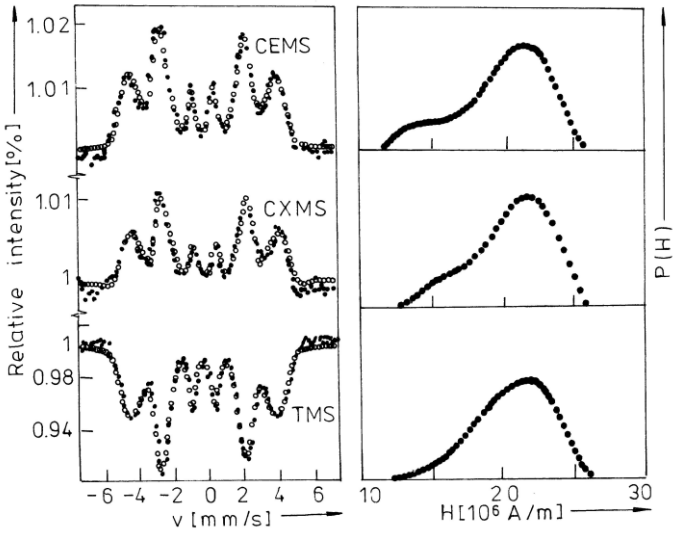

Fig. 6. CEMS, CXMS and TMS spectra and their hyperfine distribution after rf exposure to radiofrequency power of 25 W.

Rf annealing induces different surface short-range ordering effects in the spectra before any crystalinity could be evidenced. The quadrupole pattern relative intensity in CEMS spectra was suggested as possible monitor of this behavior. The quadrupole distribution was assigned to FeSi clusters. TMS spectra reflect the bulk stress relief under the rf annealing. A quadrupole interaction analysis reveals almost identical threshold energy for the bulk stress relief and for the chemical short-range order (CSRO) growth in the CEMS spectra. Structural relaxation, associated with boron diffusion is obtained above a threshold value of P_{rf} = 1W. An activation energy of 1.7 eV was estimated for the onset of surface CSRO in the rf annealed FeBSiC system.

Mössbauer spectroscopy was used for structural investigation of laser ablated films of nominal composition $Fe_{81}B_{13.5}Si_{3.5}C_2$ starting from cast ribbon targets of Metglass 2605 SC [37]. The CEMS spectra were obtained for ribbon target and ablated films. Film spectra show a line broadening of the amorphous pattern compatible with a decrease in average grain size compared with the ribbon target, Analysis of the hyperfine field distribution at Fe sites indicates a 23% content in nano-sized particles in the ablated films, with the particles having an estimated average grain of about 15 nm. Deconvolution of the hyperfine field distribution curve of CEMS spectra indicates that the ablated films contain about 23% nano-sized grains, which could provide a basis for an improvement in the soft properties.
The crystallisation process of the $Fe_{87}Zr_6B_6Cu_1$ sample has been studied by means of TMS, CEMS and X-ray diffraction [38]. $Fe_{87}Zr_6B_6Cu_1$ amorphous ribbon was obtained by the melt spinning technique. The surface of the as-quenched ribbon was subsequently polished to remove any possible residual surface crystal. One-hour isothermal treatments at 350, 475 and 575°C were performed in a differential thermal analyser apparatus. The experimental results show different grades of crystallisation depending on the depth of the layer studied. The crystallisation process begins on the surface of the sample and extent with annealing temperature to the interior the sample.
The effect of high-energy beam and pulsed excimer laser irradiation on magnetic properties of $Fe_{80}B_{20}$ amorphous alloy was studied for direct comparison [39]. Both types of irradiation were found to induce changes in the magnetic anisotropy dependent on the values of the irradiation parameters. While the effect of high-energy electron beam irradiation was weaker, pulsed excimer laser irradiation was found to induce, through a suitable selection of irradiation parameters controlled changes in the magnetic anisotropy and/or relaxation of quenching stresses. Due to magneto elastic effects, the in-plane domain structured of the non irradiated foil was changed by the laser treatment performed to a closure structure.
The amorphous to crystalline transformation of $Fe_{62}Ni_{16}B_{14}Si_8$ under isothermal annealing at the crystallization temperature T_x = 720 K was investigated [40]. During the annealing the onset of crystallization at the surface before the bulk was evidenced by the reorientation of magnetic anisotropy perpendicular to ribbon plane and by the annealing time dependence of the mean hyperfine field value. The crystallization process was found to occur in two steps: a metastable equilibrium of the amorphous phase with the precipitated bcc-(FeNi), bcc(FeNi)Si and bct-$(FeNi)_3B$ phases, followed by the decomposition of meatastable bct--$(FeNi)_3B$ into the stable $(FeNi)_2B$ and bcc-(FeNi) final crystalline phases. Partial Fe substitution by Ni atoms leads to the increase of the mean magnetic moment at the iron sites.

5. Thin films of Cu and Ag doped with ^{57}Fe

There is growing interest in the magneto-transport properties of heterogeneous granular alloys formed by small particles of a ferromagnetic metal dispersed into a non-magnetic metallic or insulating matrix.

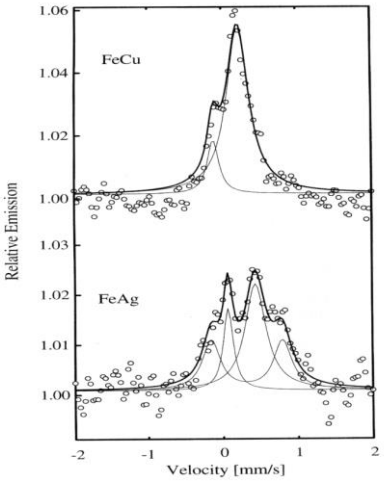

Fig. 7. CEMS spectra of diluted granular films of Cu-Fe and Ag-Fe (iron content ≤ 2%) produced using ^{57}Fe implantation Cu (Ag) films, previously grown by laser ablation.

Were reported results on granular films with ^{57}Fe implanted into Cu and Ag (iron content ≤ 2%) films grown by pulsed laser deposition. The local structure of the implanted iron was evidenced by CEMS spectra analysis [41]. Figure 7 shows the CEMS spectra recorded at room temperature. The singlets having isomer shifts IS = 0.25 mm/s in Cu and 0.5 mm/s in Ag are likely to be due to individual Fe atoms dissolved in the FCC Cu or Ag matrices surrounded by 12 nearest-neighbour Cu (Ag) atoms. The large width suggests that Fe atoms be situated at damaged regions of the lattice. This appears as the dominant Fe phase in Fe/Cu film representing 85% of the total amount of iron in this film. For the Fe/Ag film this phase contributes only with 46% of the total iron amount. In fact, for the Fe/Ag film we observed an additional doublet in the CEMS spectrum, here assigned to iron atoms dissolved in Ag, but having one or more Fe atoms amongst its 12 nearest-neighbours. The presence of both Fe and Ag atoms in this shell destroys the cubic symmetry at the central iron site resulting in a large quadrupole splitting QS = 1.1 mm/s. From the relative intensity of the QS-doublet we estimate that 37% of the iron ions in Fe/Ag are in this non-symmetric phase. Thus, for the Fe/Ag film we obtain a relative content of 83% of iron atoms dissolved in the Ag matrix (therefore, in no ferromagnetic state) by summing the contributions from the singlet with 46% relative intensity and the doublet with 37% relative intensity. The presence of the quadrupole interaction in the silver matrix film also indicates a less packed structure that than of the copper matrix. Finally, the singlets at IS $= -0.13$ mm/s in Fe/Cu and 0.08 mm/ in Fe/Ag have isomer shifts close to that of metallic iron and hence are assigned to sufficiently large Fe clusters where each Fe atom has 12 Fe nearest neighbours as in the BCC structure of normal α-Fe. It was reasonable to assume that the six-line pattern expected from metallic iron is not seen here (our measurements were done at room temperature) because the Fe

clusters exhibit superparamagnetic relaxation and the six-line pattern then collapses into a singlet. This metallic Fe phase has a relative intensity of 15% in the Fe/Cu film and 17% in the Fe/Ag film. In Cu and Ag films implanted with ^{57}Fe ions (Fe content $\leq$ 2%), Mössbauer spectra by conversion electrons show that Fe forms either small clusters (of a few atoms), the dominant phase in the Cu film (85% of total Fe) or large α-Fe particles (15% of total iron for the Cu film, respectively 17% for the Ag film).

6. Sn compounds

Tin and its compounds (like chalcogenides, etc) have strong implications in many applications. ^{119}Sn Mössbauer spectroscopy is a very efficient tool for probing the local environment of tin atoms and their intercalation products. The following compounds were investigated: β-tin foil, tin layers deposited by electrochemical method, [42] chalcogenide $SnSe_2$ [43], $SnSe_2Ag_x$ system [42], xSnO2-[(1-x)[α-Fe2O3] nanoparticle system [44].

$SnSe_2$, bulk samples, was prepared by mixing corresponding amounts of Sn and Se powder (high purity grade) in sealed quartz ampoule. The films were deposited by two methods: PLD (pulsed laser deposition deposition was carried out with a KrF excimer laser) and PED (pulsed electron deposition was made with electron beams produced in channel-spark discharge deposition methods). Mössbauer measurements were performed by transmission (TMS), respectively conversion electron spectroscopy (CEMS). Some spectra are presented in figure 8. The spectral parameters of the Mössbauer components of each spectrum, are given in Table 1. In the table are indicated the compounds corresponding to each subspectrum. Mössbauer parameters for $SnSe_2$ bulk samples are the same as in literature. There is an oxidation process on their surface indicated by the presence of the SnO_2 oxide in the CEMS spectrum of the bulk sample. The structure of main component of the films it is possible to be built from isolate $SnSe_4$ tetrahedra stabilized by atoms occupying intermediated positions. SnSe there is present in the both films in a small amount. On the film obtained by PLD deposition we found SnO_2 oxide. We consider that by PED deposition method a better film is obtained

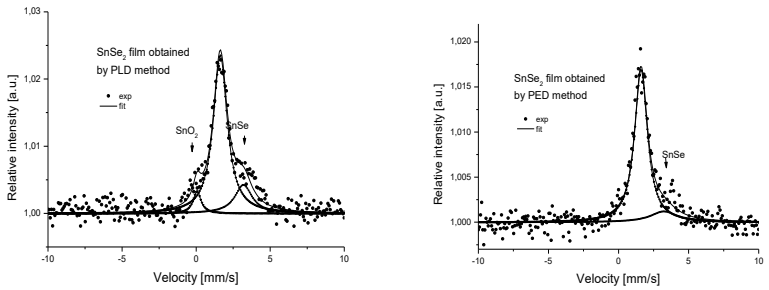

Fig. 8. Conversion electron Mössbauer spectroscopy spectra of $SnSe_2$ films obtained by PLD and PED deposition.

Table 3. The spectral parameters of the Mössbauer spectra presented in Fig. 8

Sample	IS [mm/s}	W [mm/s]	ε %	A %	Assigned compound
$SnSe_2$ - bulk	1,43	0,90	4,78	100	$SnSe_2$
$SnSe_2$ - surface	1,40 0,05	0,86 1,16	8,07 0,86	87,09 12,91	$SnSe_2$ SnO_2
$SnSe_2$ film obtained by PLD method	1,69 3,28 0,07	1,15 1,43 0,85	2,35 0,44 0,34	76,98 16,86 6,23	$SnSe_4$ SnSe SnO_2
$SnSe_2$ film obtained by PED method	1,65 3,32	1,12 2,32	1,71 0,12	87,65 12,35	$SnSe_4$ SnSe

where:
IS: Isomer shift in mm/s; errors ± 0.02; W: Line width in mm/s; errors ± 0.03; ε: Resonant effect in %; errors ± 0.05; A: Relative area of each subspectrum in %; errors ± 4

The backscattering measurement of β-Sn foil evidenced presence of the SnO_2 on the sample surface; this fact was not possibly for transmission measurement. The thickness of the SnO_2 film was estimated to 4 nm. The isomer shift, easily different of SnO_2 reference sample, shows a change in its stoichiometry.
The tin layers were electrochemically deposited on carbon steel surface from acidic baths of tin chloride. Mössbauer spectroscopy shows that the tin layers contains metallic tin and tin oxide, in different proportions and these proportions are strongly dependent of deposition current. Parameters for metallic tin are identically with those of the reference sample. The tin oxide parameters are easily different from those of the reference sample, explained by small differences of tin oxide crystalline structure for electrodeposited layers. We considered that tin oxide is situated on the surface of the deposited tin layer.
During the last years a special attention has been paid to semi-conducting oxides in order to apply heir sensing properties in detection of the toxic or dangerous gases. The components of $xSnO_2$-(1-x)αFe2O3 oxide family are promising gas sensing materials. The $xSnO_2$-(1-x)αFe_2O_3 nanoparticle system was investigated. [44], [45], [46]. A structural transition, implying the change of lattice dynamics characteristics have been detected for $0,4<x<0.5$. Under $x \approx 0.3$ a superposed of tree distribution of magnetic fields was revealed. The effect of the grain size and the near-neighbor interactions compete to distribution of magnetic fields. Under $x \approx 0,125$ the mainly contribution to distribution of magnetic fields is given by the near-neighbor interactions and local disorder. Distributions of magnetic fields at low x values have been associated with different local vicinity of ^{119}Sn in α-Fe_2O_3.
Also SnO_2 is an attractive host lattice for the investigation of diluted magnetic semiconductors as materials for spintronic applications.

7. Eu compounds

Were performed surface measurements and transmission measurements for samples containing ^{151}Eu Mössbauer isotope [47]. I believe that electrons surface

measurements through ^{151}Eu are a world first, in my opinion. I demonstrated theoretical and experimental the possibility to do surface measurements on sample containing ^{151}Eu for practically the same depth range as for isotopes ^{57}Fe, ^{119}Sn by detecting Auger electrons. The backscattering measurements by detection of X-rays were performed for the first time in Romania.

In the last years increased the number of studies with ^{151}Eu isotope for a large class of materials: advanced optical materials (with special properties) based on crystals YAG, YVO_4, LGS doped with Eu, glass materials, special ceramic materials (Pb-Ti doped with Eu).

The morphological changes induced by the thermal treatments of YAG: Eu crystals synthesized by a sol-gel method have investigated using the Mössbauer and optical techniques [48]. The YAG:Eu nanocrystals were obtained by a nitrate-citrate sol-gel method. Mössbauer measurements performed at room temperature on powder samples annealed at 900, 930, 1000, 1100, 1200, 1300, and 1400. The Mössbauer spectra (MS) are shown in figure 9. Spectrum of the sample annealed at 900°C shows a central peak and an additional one at ~ + 7mm/s, which has not found in the other spectra. Mössbauer spectra for the samples annealed at $T_{an} \geq 930$°C evidence a very large and slightly asymmetric transmission peak closed to center. The obtained Mössbauer parameters are showing abrupt changes from $T_{an} = 900$°C to $T_{an} = 930$°C (known as amorphous-crystalline temperature of YAG). The sudden changes of observed parameters of the samples annealed at 900^0C and 930^0C most probably correspond to the amorphous crystalline transformation of YAG. The MS of samples annealed at $T_{an} > 930^0$C revealed slower changes of spectral parameters vs. increasing T_{an}. The slow changes of the Mössbauer spectral parameters can be explained taking into account the contributions of the Mössbauer probes on crystallite boundary (surface) and in volume one to spectra. The growth of crystallite and the increasing of its apparent average size induce an increasing of all MS parameters go to their limit-values. All data for the spectra annealed at $T_{an} \geq$ 930°C evidence the presence of trivalent state of the Mössbauer hosting ion in a neighborhood with a very slight distortion of oxygen polyhedrons, corresponding to a high symmetric location of the Mössbauer probe. Taking into account the geometrical aspects the electric charge balance and the chemical similarity of the Y and Eu properties, the ionic host of Mössbauer probe is substituting the Y in the Thompson cube of YAG crystal.

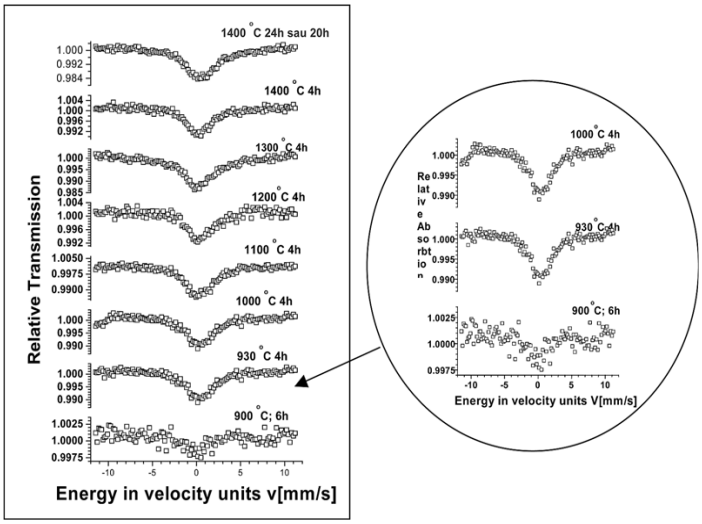

Fig. 9. Mössbauer spectra of the YAG:Eu sample annealed at specified annealed temperatures.

$YVO_4:Eu^{3+}$-nanocrystals (with nominal 5 at.% Eu), strong luminescent material, have been obtained by the precipitation procedure. Mössbauer measurements were performed at room temperature in transmission and backscattering geometry by electron detection [49], [50]. Up to 700^0 C, the Mössbauer spectra consist in two main contributions: a central broad as preponderant line-resonance (A) and a less large and less intense resonance (B), around v∈ [5 mm/s ÷ 6 mm/s]. This behaviour can be ascribed to the presence of Eu ions in different possible micro-environments in YVO4:Eu structure. The two different micro-environments of ^{151}Eu correspond to different distorted oxygen polyhedrons of trivalent Eu-ions. As the annealing temperature increases, the B contribution intensity decreases up to its disappearance and A becomes more symmetric at T_o ~700°C. Mössbauer parameters of backscattering spectra suggest a higher distortion of the Eu neighborhood at surface. The best fit for the sample annealed at T> 700^0C has one pattern. The temperature dependence of the Mössbauer line-shapes of spectra suggests the effect of nanocrystals growth vs. annealing temperature. The fit results for the annealed samples revealed a critical temperature $T_o \approx 700\ ^0$C, suggesting a transition state in the growth process of YVO_4:Eu crystallite.

Trigonal crystals with disorted Ca-gallogermanate structure also have attracted attention due potential applications. Among these, the langasite (LGS) crystals ($La_3Ga_5SiO_{14}$) are widely used in acoustical applications. The structure of the Eu centers in the langasite crystal was investigated [51]. LGS crystals doped up to 5 at % were made in the same conditions as undoped crystals. The effect of the static-disordered nature of crystals fields surrounding the europium probe in crystal was detected. The spectrum suggested different chemical bonds Eu-O and different surrounding of the Mössbauer nuclide in doped crystal. The best fit of the spectrum indicated that Mössbauer nuclide has two distinct two vicinity, approximately cubic vicinities and characterized by small electric field gradient quadrupolar. The

presence of the vicinities is due the random distribution of Si^{4+} and Ga^{3+} in the D sites. All results show that the LGS crystals are europium doped and Eu^{3+} enter A site.

8. Conclusions

The paper convincingly presents a large part of the scientific contributions in the study of materials by Mössbauer spectroscopy obtained by the author in the over 40 years of activity in scientific research, alone or in collaboration. The contributions, made in the vast majority entirely by Romanian authors, are exemplified by numerous scientific papers published in prestigious journals from abroad and in the country. The studies carried out show that Mössbauer Spectroscopy is a very effective method in the study of different materials, especially in the case of ferrous materials. For a better understanding of material properties, a correlation of the Mössbauer results with those obtained by other methods is useful and necessary.

References

[1] Mössbauer R.-L., *Nuclear resonance fluorescence of gamma radiation in $^{191}Ir.$*, Z. Phys., **151**, 1958, p. 124–143.
[2] Long G. J. and Grandjean F., (Eds.), *Moessbauer Spectroscopy Applied to Magnetism and Materials Science*, vol. 2, Plenum, Dordrecht, 1996.
[3] Maddock A. G., Moessbauer Spectroscopy: Principles and Applications of the Techniques, Horwood Chemical Science Series, Horwood, Chister, 1997.
[4] Bibicu I., *Mossbauer spectroscopy applied to surface study*, Revue Roumaine de Chimie, **57**, 9-10, 2012, p. 877-889.
[5] Bibicu I., *Mössbauer studies on steel samples*, Journal of Engineering Sciences and Innovation, **6**, 3, 2021, p. 289 – 306.
[6] Barb D., Morariu M., Tarina D., Bibicu I., Constantinescu S., Diamandescu L., *Utilizarea efectului Mössbauer in studiul proprietatilor unor oteluri industriale Fe-C, St. Cerc*. Fiz., **25**, 1973, p. 17- 26.
[7] Barb D., Morariu M., Diamandescu L., Bibicu I., *Internal magnetic fields in Fe-Si electrotechnical steels*, Rev. Roum. Phys., **19**,1974, p. 425-429.
[8] Meisel, W., *Hyperfine Interactions*, **111**, 1-4, December 1998, p. 59-70.
[9] Bibicu I, *The study of corrosion through the Mössbauer effect is a small step towards a sustainable development in harmony with nature*, Journal of Engineering Sciences and Innovation, **10**, 2, 2025, p. 167 – 180
[10] Bibicu I., Moisil G.C., Barb D., Romanescu M., *Mössbauer technique for investigation the action of an anorganic inhibitor of corrosion*, Rev.Roum .Phys., **20**, 1975, p. 531-535.
[11] Bibicu I., Bulea C., Diamandescu L., Rus V., Popescu Tr., Mercioniu I., *Characterization of surface and interface of Fe-C steel under electrolytic galvanization*, Proceedings of the Romanian Academy - series A; **19**, 3, 2018, p. 423-430.
[12] Bibicu I., Nicolescu G., Cretu C., *Hyperfine Interactions, A versatile gas-flow proportional counter for Mössbauer spectroscopy*, **192**, 1, 2009, p. 85-91; DOI: 10.1007/s10751-009-9950-7.
[13] Bibicu I., Samide A., M. Preda, *Steel corrosion in diluted ammoniac solutions studied by Mössbauer spectrometry*, Mat. Lett., **58**, 2004, p. 2650-2653.
[14] Samide A., Bibicu I., Rogalski M., Preda M., *Surface study of the corrosion of carbon steel in solutions of ammonium salts using Mössbauer spectrometry*, J. Radioanal. Nucl. Chem., **261**, 2004, p. 593-596.

[15] Samide A., Bibicu I., Tutunaru B., Preda M., *Studiul suprafetei oţelului-carbon corodat in ape industriale care contin NH_3/NH_4Cl utilizând spectrometria Mössbauer*, Rev. Chim-Bucharest, **56**, 2005, p. 850-853.
[16] Samide A., Bibicu I., Rogalski M., Preda M., *A study of the corrosion inhibition of carbon-steel in dilluted ammonia media using 2-mercapto-benzothiazol (MBT) by Mössbauer spectrometry*, Acta Chim. Slovenica, **51**, 2004, p. 127-136.
[17] Samide A., Bibicu I., Rogalski M. S., Preda M., *Surface study of the corrosion inhibition of carbon steel in diluted ammonia media using N-ciclohexil-benzothiazole-sulphenamida*, Corrosion. Science., **47**, 2005, p. 1119-1127.
[18] Samide A., Bibicu I., Rogalski M., Preda M., *Studiul inhibării coroziunii oţelului-carbon cu etilentiouree în soluţii de clorură de amoniu utilizând spectrometria Mössbauer*, Rev. Chim-Bucharest, 54, 2003, p. 927-931.
[19] Patru A., Bibicu I., Agiu M., Preda M., Tutunaru B., *Mossbauer Spectroscopy study on the corrosion inhibition of carbon steel in hydrochloric acid solution*, Mater. Lett., **62**, 2008, p. 320-322.
[20] Samide A., Bibicu I., Turcanu E., *Corrosion inhibition of carbon steel in hydrochloric acid using n-acetyl p-aminobenzene sulfonamide*, Rev. Chim-Bucharest, **60**, 2009, p. 564-567.
[21] Samide A., Bibicu I., Turcanu E., *Surface analysis of inhibitor films formed by N-(2hydroxybenzilidene) thiosemicarbazide on carbon steel in acidic media*, Chem. Eng. Commun., **196**, 2009, p. 1008-1017.
[22] Samide A., Bibicu I., *A new inhibitor for corrosion of carbon steel in hydrochloric acid solution*, Rev. Roum. Chem., **54**, 2009, p. 33-43.
[23] Samide A., Bibicu I., *Kinetics corrosion process of carbon steel in hydrochloric acid in absence and presence of 2- (cyclohexylaminomercapto) benzothiazole*, Surf. Interface Anal., **40**, 2008, p. 944-952.
[24] Tutunaru B., Pătru A., Bibicu I., Preda M., *The study of the passive film formed on the surface of 316L stainless steel in artificial physiological media*, J. Optoelectron. Adv. Mater, **9**, 11, 2007, p. 3400-3404.
[25] Samide A., Bibicu I., Oprea B., Cioatera N., Ciuciu A., *The study of passive film formed on 316L stainless steel Surface for orthopedic implant applications*, Journal of Optoelectronics and Advanced Materials, **10**, 6, 2008 p. 1431-1436.
[26] Bibicu I., Samide A., Oprea B., Tutunaru B., *The study of passive film formed on 316L stainless steel Surface for orthopedic implant applications*, Journal of Optoelectronics and Advanced Materials, **10**, 8, 2008 p. 2156-2158.
[27] Amado M.M., Rogalski M.S., Guimaraes L., Sousa J.B., Bibicu I., Welch R.G., Palmer S.B., *Magnetic properties of NiZn and MnZn ferrite films deposited by laser ablation*, J. Appl. Phys. 83 (11), 1998, p. 6852 – 6854.
[28 Feder M., Diamandescu L., Bibicu I., Caltun O.-F., Vilceanu V., *On the sintering properties of Ni-Zn ferrite with Cu substitution, Proceedings of the XWRTCS*, Science of Sintering: Current Problems and New Trends, Serbian Academy of Sciences and Arts, Beograd, 2003, p. 397-403.
[29] Feder M., Diamandescu L., Bibicu I., Caltun O.F., Dumitru I., Boutiuc L., Chiriac H., Lupu N., Vilceanu V., Vilceanu M., *Comparative study on the microstructural and magnetic properties of cobalt ferrites synthesized by ceramic and oxidation wet methods*, IEEE Transactions on Magnetics, **44**, 11, 2008, p. 2936-2939, DOI: 10.1109/TMAG.2008.2002200.
[30] Caltun O.F., Dumitru I., Feder M., Diamandescu L., Bibicu I., Vasiliu F., Lupu N., Vilceanu V., *The influence of chemical composition on magnetic properties and magnetostriction coefficient of cobalt ferrites*, Journal of Optoelectronics and Advanced Materials, **10**, 7, 2008, p. 1775-1778.
[31] Dippong T., Levei E.A., Diamandescu L., Bibicu I., Leostean C., Borodi Gh., Tudoran L.B., *Structural and magnetic properties of Co_XF_{3-X} O_4 versus CO/Fe molar ratio*, Journal of Magnetism and Magnetic Materials, **394**, 2015, p. 111-116.
[32] Dippong T., Cadar O., Levei E.A.,Bibicu I., Diamandescu L., Leostean C., Lazar M., Borodi Gh., Tudoran L. B., *Structure andmagnetic properties of $CoFe_2O_4$-SiO2 nanocomposites obtained by sol-gel and post annealing pathways*, Ceramics International, **43**, 2, 2017, p. 2113-2122 (2016).
[33] Rogalski M., Bibicu I, *Surface short range order induced by RF annealing $Fe_{81}B_{13.5}Si_{3.5}C_2$ glass*, Mater. Lett., **13**, 1992, p. 32-34.

[34] Bibicu I, Rogalski M. S., Nicolescu G., *Transmission and conversion electron Mössbauer investigation of $Fe_{81}B_{13.5}Si_{3.5}C_2$ glass under RF thermal treatment*, Phys. Stat. Sol. (b),**178**, 1993, p. 459-464.
[35] Rogalski M. S., Bibicu I., Sorescu M., *CEMS investigations of surface hyperfine interactions in $Fe_{81}B_{13.5}Si_{3.5}C_2$ glass*, Hyperfine Interact., **92**, 1994, p. 1317-1321.
[36] Rogalski M. S., Bibicu I., *CEMS, CXMS and transmission Mössbauer investigation of the RF isochronal annealing of $Fe_{81}B_{13.5}Si_{3,5}C_2$glass*, Physica Stat. Sol (b), **195**, 1996, p.531-536.
[37] Rogalski M. S., Jackson T. J., Bibicu I., Palmer S. B., *Deposition of $Fe_{81}B_{13.5}Si_{3.5}C_2$ films by excimer laser ablation and their structural investigation*, J. Phys. D Appl. Phys., **27**, 1994, p. 2167-2170.
[38] Bibicu I., Garitaonandia S., Plazaola F., *Apinanz E., X-ray diffraction, transmission Mössbauer spectrometry and conversion electron Mössbauerspectroscopy studies of the $Fe_{87}Zr_6B_6Cu_1$ nanocrystallization process*, Journal of Non-Crystalline Solids, **287**, 2001, p. 277-281.
[39] Sorescu M., Knobbe E. T., Barb D., Sorescu D., Bibicu I., *Comparison of electron beam and pulsed laser irradiation effects in $Fe_{80}B_{20}$*, Hyperfine Interactions, **92**, 1994, p.1347-1353.
[40] Barb D., Bibicu I, Rogalski M. S., Sorescu M., *Mössbauer investigation of amorphous to crystalline transformation of $Fe_{62}Ni_{16}B_{14}Si_8$by isothermal annealing*, Hyperfine Interactions, **94**, 1994, p. 2187-2192.
[41] Pereira de Azevedo M. M., Sousa J. B., Mendes J. A., Almeida B. G., Rogalski M. S., Pogorelov Yu. G., Bibicu I., Redondo L. M, da Silva M. F., Jesus C. M., JMarques. G., Soares J. C., *Magnetization and magnetoresistance in Fe-ion-implanted Cu and Ag thin films,* J. Magn. Magn. Mater., **173**, 1997, p. 230-240.
[42] Bibicu I., *Mössbauer surface studies of tin and some tin compounds*, Proceedings of VI-th International Conference: days of the Academy of Technical Science from Romania, ISSN 2066-6586, Timisoara, Romania, 22-23 September 2011, Part 1/B5/p. 154-159.
[43] Bibicu I.., Lőrinczi A., Velea A., Sava F., Popescu M., *Structure and Mössbauer measurements on $SnSe_2$ bulk and thin films*, Optoelectronics and Advanced Materials-Rapid Communications, **4**, 10, 2010, 1568-1571.
[44] Constantinescu S., Diamandescu L., Bibicu I., Tarabasanu-Mihaila D., Feder M., *Hyperfine interactions and dynamics characteristics of ^{119}Sn in $xSno_2$-(1-x)α-Fe_2O_3 nanoparticle system*, Hyperfine Interact, **184**, 2008, p. 83–89.
[45] Diamandescu L., Constantinescu S., Tarabasanu – Mihaila D., Bibicu I., Feder M., Vlaicu M. A., Mössbauer investigation of hyperfine interactions in dilute Fe-SnO_2 nanoparticles, Journal of Physics: Conference Series **217,** 2010, article number: 012110, doi:10.1088/1742-6596/217/1/012110.
International Conference on the Applications of the Mössbauer Effect (ICAME 2009) IOP Publishing.
[46] Constantinescu S., Diamandescu L., Bibicu I., Tarabasanu-Mihaila D., Feder M., *^{119}Sn- and ^{57}Fe Mössbauer investigation of xSnO2-[(1-x)[a-Fe2O3] nanoparticle system*. (I) *Magnetic hyperfine field distribution in Sn-low dilute system*, Rom. Journ. Phys., **56,** 5-6, 2011, p. 692-697.
[47] Bibicu I., *Some comments on ^{151}Eu Surface Mössbauer Spectroscopy*, Eur. Phys. J. Appl. Phys., **62**, 1, 2013, 11302 (3 pages) Doi: http://dx.doi.org/10.1051/epjap/2013120328.
[48] Constantinescu S., Georgescu S., Bibicu I., Chimie A.M., Stefan A., Toma O., *Mössbauer and optical investigation of Eu:YAG nanocrystals synthesized by a sol gel method*, Rom. Journ. Phys., **52**, 3-4, 2007, p. 295-307.
[49] Bibicu. I., Constantinescu S., Diamandescu L., Voiculescu A. M., Cotoi E., *Mössbauer spectroscopy study on YVO_4:Eu luminescent material*, Rom. Rep. in Phys., **66**, 4, 2014, p. 1012-1017.
[50] Voiculescu A. M., Cotoi E., Toma O., Georgescu S., Constantinescu S., Bibicu I., *Optical and Mössbauer spectroscopy studies on YVO_4:Eu nanophosphor*, Romanian Reports in Physics, **62**, 1, 2010, p. 121–127.
[51] Constantinescu S., Gheorghe I., Stoicescu C., Georgescu S., Toma O., Bibicu I., *Growth and XRD, optical and Mossbauer investigations of Eu doped trigonal La-Gallosilicate crystal*, Rom. Rep. Phys., **57**, 2, 2005, p. 249-260.